

High Energy Density Science with X-ray Free-Electron Lasers

J. S. WARK⁽¹⁾

⁽¹⁾ *Department of Physics, Clarendon Laboratory, University of Oxford, Parks Road, Oxford, OX1 3PU, United Kingdom*

Summary. — Extreme states of matter with high temperatures and pressures can be created by irradiating matter with either intense X-Rays emitted by X-Ray free-electron-lasers (FELs), and by heating and/or compression with optical lasers and then using the FEL X-Rays as a probe. We provide here a very basic introduction to this burgeoning field, highlighting a few specific experiments, and signposting some directions for future exploration.

1. – Introduction

By convention the term ‘High Energy Density’ (HED) has come to be used to denote those regions of the phase diagram of matter with energy densities in excess of order 10^{11} Jm^{-3} [1], which equates to a little over 0.6 eV \AA^{-3} . From this latter measure we immediately see that part of this research field is concerned with matter at ion densities similar to those found in solids (with each atom occupying a few cubic \AA) but heated to temperatures in the multi-eV region. Recalling that room temperature equates to $1/40^{\text{th}}$ eV, and 1 eV is equivalent to of order 11,000 K, we note we will be dealing with dense plasmas with conditions (in terms of densities and temperatures) comparable to those found as we travel towards the centre of the sun, giant planet or other dense astrophysical object.

As well as increasing the internal energy of an object by heating, HED conditions can also be achieved by compression. For example, a typical cold metal needs to be subject to a pressure of several million atmospheres (Mbar) to have its volume halved. As 1 Mbar is approximately 10^{11} Nm^{-2} during such compression the work performed per unit volume, $P\Delta V/V$ must thus itself be of order 10^{11} Jm^{-3} – our original definition of the onset of the borders HED science (HEDS).

Generally speaking, therefore, we will be concerned with matter of order solid density or greater, that has either been heated or compressed (or both), engendering high energy density. Whilst clearly such energy densities can also be given to matter with far low densities than those of solids, by heating them to even greater temperatures, for reasons that will be explained below those sorts of conditions have not yet attracted as much interest to those in the HEDS community using free electron lasers.

These notes – designed as an extremely basic introduction for non-specialists in the field – are thus divided roughly into two halves: the first outlining the physics and interest in solid density matter heated to high temperatures, and the second to matter subjected to high compressions. In each case we will consider the basic physics of interest, the motivation for studying such systems, and the revolutionary impact that x-ray free-electron-lasers (FELs) are having in these burgeoning areas of science. As we explore matter in these two regimes, it will be useful on occasion to refer to Fig. 1 where we plot some features of the phase diagram of aluminium (as an example) as a function of temperature and pressure.

X-Ray free electron lasers (FELs) are used in this field in two main ways. Firstly, the energy within a typical 100-fsec pulse (of order a few mJ) is such that when the FEL output is focussed down to a small spot (of order a micron in diameter), the intensities are in the region of 10^{17}Wcm^{-2} , and the electrons within a solid can be heated, at least in the case of softer x-rays, to temperatures of order a few hundred eV before the ions have time to significantly move. This constitutes the warm dense matter (WDM) and dense plasma region shown in Fig.1. We consider what can be learnt from such an experiment in section 3. Secondly, systems can be compressed and heated by optical lasers, where an intense optical pulse ablates plasma away from the surface of a target, and the resultant pressure pulse launched into the bulk of the material is such that the pressures reached can, in principle, exceed those generated by static techniques (though FEL experiments themselves have yet to attain that goal). As we shall find in section 5, at pressures in the region a

couple of Mbar or below, the material remains solid, and the advantage of the FEL is that it can be used to obtain a diffraction pattern from the compressed crystal on a timescale that is shorter than even the fastest phonon period. We will consider such experiments in subsections 5.2 and 5.3, where the high quality diffraction patterns now obtained have provided novel insight into how materials deform as they are rapidly compressed, and have demonstrated that complex phase transformations in the solid state can take place on the nanosecond timescales of the optical laser compression pulses. As the transient pressures induced by laser compression increase, the heating induced by the shock can melt the sample, entering the dense plasma regime. We discuss such experiments in section 6. Finally, in section 7, we muse upon future directions, given improvements in both the parameters of the FELs, and of the optical lasers coupled to them.

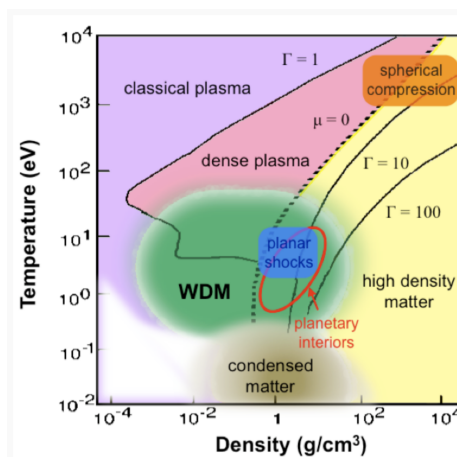


Fig. 1.: Regions of the phase diagram of aluminium ($Z = 13$). To the bottom right of the line $\mu = 0$ the plasma is Fermi degenerate, and to the bottom right of the line $\Gamma = 1$ it is strongly coupled (as defined by the ion-ion coupling parameter).

2. – Dense Plasmas

As noted in the introduction, HEDS encompasses both dense plasmas and highly compressed solids. To take dense plasmas first, we have already noted that they are of interest as they are so prevalent throughout the universe – it is an oft-quoted figure that more than 99 % of all visible matter in the universe is in the plasma state, given that nearly everything we can see in the night sky is in this form. However, they are also of interest from a purely theoretical point of view, in that they are very difficult to model compared with a so-called classical plasma (the top left hand region of Fig.1). This difficulty arises because they are often *strongly-coupled*, where the coupling parameter is taken to be a measure of the typical Coulomb energy to the typical thermal energy (a fraction which is small for a classical plasma).

In order to see this, we must first appreciate how we model a classical plasma. As we subject heat to a solid it melts, and then vaporises. If we supply yet further heat, the energy is sufficient to remove electrons from the atoms, resulting in a plasma of interacting positive ions and electrons. As noted above, a so-called classical plasma is weakly-coupled: we assume that the thermal energy greatly exceeds the coulomb energy, and to zeroth order we can treat the system as an ideal gas, only slightly perturbed by the coulomb interactions. That the plasmas of interest are not classical is such an important point that it is worth emphasising the important physics that pertains in the classical case, so as to gain insight into what knowledge we are losing in the dense-plasma case. Consider a hot, sparse plasma of protons and electrons both at a temperature T , which is overall neutral such that the mean electron density equals the mean ion density, n_0 . Into this plasma we introduce a positive test charge, Q . Electrons will be attracted to the test charge (flying past it because they have high thermal energies), but at a distance r from the test charge there will be, on average, a few more electrons than the average number n_0 , and this excess number density we denote $n_e^+(r)$. By similar reasoning there will be a deficit of protons of the same extent, and thus a distance r from the test charge there will be an excess charge density of $\rho(r) = -2en_e^+(r)$. This excess charge density gives rise to a potential, $\phi(r)$, and the electrons have potential energy $-e\phi(r)$. We assume that the electrons are obeying Boltzmann statistics, so the excess number density with this energy scales as $n_0(\exp[e\phi(r)/k_B T] - 1) \approx n_0 e\phi(r)/k_B T$, where we have used our original assumption that the system is weakly coupled (i.e. $e\phi$ is small compared with $k_B T$). The above argument leads us to conclude that around the test charge we have a charge density given by

$$(1) \quad \rho(r) = -\frac{2n_0 e^2 \phi(r)}{k_B T} \quad .$$

However, we know that Poisson's equation must also be obeyed: that is to say

$$(2) \quad \nabla^2 \phi(r) = \frac{1}{r} \frac{\partial}{\partial r} \left(\frac{1}{r} \frac{\partial \phi}{\partial r} \right) = -\frac{\rho(r)}{\epsilon_0} = \frac{2n_0 e^2}{\epsilon_0 k_B T} \phi(r) \quad .$$

The above equation has the solution

$$(3) \quad \phi(r) = \frac{A}{r} \exp \left(-\frac{\sqrt{2}r}{\lambda_D} \right) \quad ,$$

where

$$(4) \quad \lambda_D = \sqrt{\left(\frac{\varepsilon_0 k_B T}{n_0 e^2}\right)} \quad ,$$

and A is a constant. Clearly at the origin the potential must simply be that due to the original test charge, Q , which fixes the constant, yielding the final solution

$$(5) \quad \phi(r) = \frac{Q}{4\pi\varepsilon_0 r} \exp\left(-\frac{\sqrt{2}r}{\lambda_D}\right) \quad .$$

The length, λ_D , is known as the Debye length, and is the typical length over which the potential due to the test charge is screened. Note that throughout this derivation we have been assuming we are dealing with the average fields due to a large number of electrons attracted to the test charge (which allowed us to use spherical symmetry to solve the problem) – we have not been considering the fields due to individual electrons and protons. Clearly for us to be able to use such an approach, there must be a large number of electrons involved in the shielding: that is to say within a sphere of radius λ_D , we must have many electrons. This dimensionless number is called the plasma parameter: the number of electrons within a Debye sphere, N_D is

$$(6) \quad N_D = n_0 \frac{4\pi}{3} \lambda_D^3 \quad .$$

It is difficult to over-stress the importance of the plasma parameter in plasma physics. A classical plasma (often called a ‘good’ plasma), is where $N_D \gg 1$, which of course is necessary for our whole approach of assuming spherical symmetry to be valid. Furthermore, although beyond the scope of these notes, we find that such plasmas are also ‘collisionless’: this does not mean that collisions between electrons and ions do not take place, but that the electrons have such high energies that in a single encounter with an ion they usually only undergo a small angle deflection, and thus need many small angle scattering events before, on average, they are deviated in angle by $\pi/2$. Indeed, we find that a typical collision time is of order N_D multiplied by the plasma period.

Thus $N_D \gg 1$ is the bedrock of classical plasma physics. However, a moment’s thought shows that this assumption does not work for the high density (and high energy density) plasmas we are discussing here. This is because the plasma parameter is also a measure of the coupling parameter. To see this we assume that each electron occupies a volume $4\pi r^3/3$, so that r is characteristic of the mean distance between particles, and then we find

$$(7) \quad N_D = n_0 \frac{4\pi}{3} \lambda_D^3 = \frac{1}{r^3} \left(\frac{4\pi r^3 \varepsilon_0 k_B T}{3e^2}\right)^{3/2} = \left(\frac{4\pi \varepsilon_0 r k_B T}{3e^2}\right)^{3/2} \approx \Gamma^{3/2} \quad ,$$

so that N_D is the ratio of the thermal energy to the Coulomb energy (raised to the power of 3/2).

Hence we find that dense plasmas, with high Coulomb coupling, have N_D of order unity or less than one, and we are not in position where we can use the inverse of the plasma parameter as an expansion parameter: thinking of the system as ideal gas-like, with coulombic interactions as being perturbations is not a valid approach. We need to

treat the thermal and potential energies on an equal footing, and this is what makes the physics of dense plasmas so difficult, and what we need to bear in mind in the sections to follow.

3. – Isochoric Heating and Ionisation Potential Depression

As discussed in the introduction, the simplest experiments using FELs to create dense plasmas involve focussing the FEL beam down to a small spot, and within the 100-fsec pulse heating the region to temperatures of a few hundred eV. It is by this means that a series of experiments have been performed to measure ionisation potentials of ions in dense plasmas.

Ions embedded in a dense plasma have lower ionisation potentials than the equivalent free ions. This phenomenon is known as ionisation potential depression (IPD). Such an effect is already present in the solid state – we know that in a metal the top of the Fermi sea in the conduction band (what a plasma physicist would think of as the start of the continuum) lies lower in energy than the final bound state in a free neutral atom. This effect influences not just the binding energies of the outermost bound electrons, but will also reduce the energy required to excite an electron from the K-shell ($n = 1$) to a state where it is free (which defines the K-edge). For example, an isolated aluminium ion which is triply ionised (so that it has 10 bound electrons) in free space would have a K-edge at 1607 eV (the energy difference for the transition $1s^2 2s^2 2p^6 \rightarrow 1s^1 2s^2 2p^6 + e$, where the free electron is at rest in the continuum). However, in the dense metal the $n = 3$ and higher states form conduction bands, and the actual energy of the K-edge is at 1560 eV, some 47 eV lower.

The question then arises as to where the continuum starts for ions in dense plasmas, and how does it vary with temperature and pressure? In the low density, hot, classical plasma regime it is assumed that the field around an ion decays exponentially according to equation (5), and this charge screening then dictates where the continuum starts. At higher densities a simpler temperature-independent approach which is often used, and which attempts to take into account the fact that an electron will not be bound if it starts to interact with the neighbouring ion, is the ion-sphere (IS) average atom model. In this model one defines a radius, R_0 of an overall-neutral sphere containing an ion of charge z^* , such that $4\pi R_0^3/3 = z^*/n_e = 1/n_i$, and then we determine the IPD to be $C_{IS} z^* e^2 / (4\pi \epsilon_0 R_0)$. where the constant C_{IS} is taken to be 9/5. [2]

With the dense IPD being temperature independent, and the classical result not so, various theories have been devised to interpolate between the two. The best known of these is the Stewart-Pyatt (SP) model [4], which although a simple classical (rather than quantum) model more than half a century old – or perhaps because of this – has been used in almost all of the atomic-kinetics calculations and codes used over the past few decades. Despite the IPD value being important in dense plasmas, as it will affect the degree of ionisation, the equation of state, the opacity etc. of the plasma, accurate measurements of it have been highly elusive, owing to the major experimental difficulty, which has dogged the field for many years, of being unable to create plasmas under sufficiently uniform conditions of temperature and density that measurements of phenomena such as IPD can be carried out with any degree of confidence. It is in this respect that X-Ray FELs have provided a step change in our capabilities. Typically, the absorption depths of solid matter to X-Rays is in the region of microns, and with 10^{12} photons in a typical pulse, when focussed to micron scale spots, the electrons within a target can be heated to of order 100 - 200 eV by the end of the 100-fsec pulse. On this timescale there is

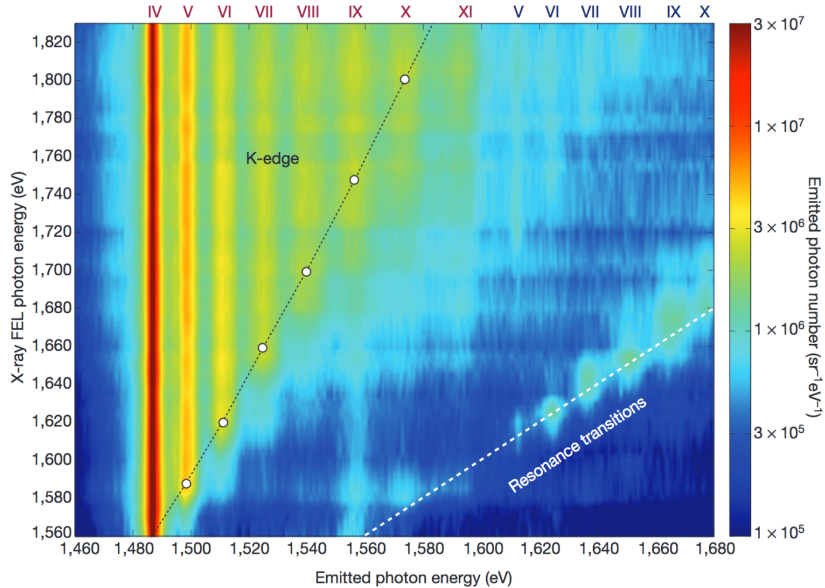


Fig. 2.: Figure from [3]. Spectrally resolved K- α emission as a function of the X-ray FEL excitation photon energy. The colour coding (bar on right) refers to the emission intensity on a logarithmic scale. Roman numerals (top) indicate the charge state of the emission peak: red, for states with a single K-shell hole; blue, for states with a double K-shell hole. Peaks around the resonance line (dashed white line, indicating where the FEL photon energy equals the emitted photon energy) correspond to emission from resonantly-pumped KL transitions. Open circles, K edges for the various charge states calculated according to a modified version of the Stewart-Pyatt model.

essentially no hydrodynamic motion, and thus the overall ion density is known exactly, and the electron density can be deduced from the dominant ion stage produced. The lack of motion is due to the fact that it will take several picoseconds for the electrons to transfer their energy to the ions, but even if that transfer were instantaneous, a 100-eV ion of Al can only move about 2-nm within the x-ray pulse length (the speed of sound is of order $\sqrt{k_B T/M} \approx 18,800 \text{ ms}^{-1}$, so in 100-fsec only a layer 2-nm thick on the surface of a target rarefies owing to expansion into the vacuum). The heating of the target during the pulse, therefore, can be safely assumed to take place at one overall density.

The experiment to perform IPD measurements with LCLS was deceptively simple [3, 5, 6]. The output from LCLS was focussed onto a 1- μm thick Al foil. The foil was heated, and gave off x-rays as described below. The photon energy of the FEL was varied between about 1460 and 1830 eV, and at each photon energy a series of shots taken (with fresh Al foil each time), to build up the x-ray spectrum (recorded by Bragg diffraction from a crystal onto a CCD) as a function of FEL photon energy which is shown in Fig. 2. In this experiment the X-Ray laser acts both as a heating pump, and as a probe. The incident FEL excites electrons from the K-shell of the ions into the conduction band (if the photon energy of the FEL is greater than the K-edge of the ion of interest). The vacancies in the K-shell are filled in two ways. The dominant pathway

is via Auger decay: an electron in $n = 2$ fills the hole in $n = 1$, and simultaneously a second $n = 2$ electron is ejected into the continuum - the transition is radiation-less. The original electron ejected into the continuum and that via Auger decay both rapidly thermalise with the other free electrons as they further collisionally ionise the system on the timescale of a couple of femtoseconds.

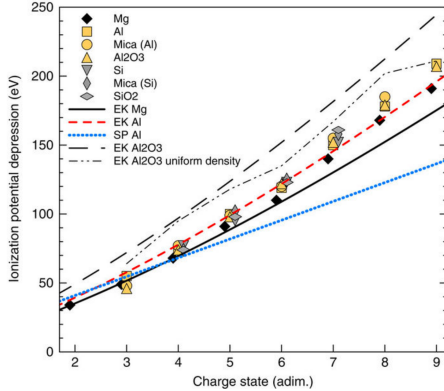


Fig. 3.: Figure from [7] The reduction in the ionization potential of Mg, Al and Si in the different materials is plotted as a function of the ionic charge state and is compared with the predictions of analytical models (EK and SP – see text), assuming a plasma ionization equal to the charge state. The data sets for each different active material are slightly shifted horizontally for clarity.

Whilst Auger decay is the common way the K-shell hole is filled, in 3% of cases (for aluminium) a photon is emitted when the $n = 2$ electron decays to $n = 1$. This is a K- α photon, and it is by recording these photons that the conditions within the solid plasma are diagnosed. As the target is heated throughout the pulse, higher and higher ionisation stages are produced. In the case of aluminium, this results in fewer electrons in the L-shell. As the L-shell population is reduced, there is less screening of both the $n = 1$ and other $n = 2$ electrons, with the result that for higher charge states the K- α photon energy shifts to higher energies for each charge state, and the K-edge of each charge state also gets larger and larger. Indeed, depending on what energy the FEL has been tuned to, it is possible for the K-edge of a particular charge state to be higher in energy than the FEL photon energy. In this case, to first order, no more electrons can be photo-ionized from the K-shell, and so K- α photons from these higher charge states are not seen.

The above description goes a long way to explaining the experimental data shown in Fig. 2. If we look at the spectrum at a particular FEL energy we only see K- α emission from those charge states with K-edges below the FEL photon energy. Alternatively, we can pick a particular charge state, and see at what FEL photon energy K- α emission from that charge state commences. Where it should commence according to the oft-used SP model is shown by the open circles in 2 – that is to say that the IPD is much greater than predicted for these conditions. Further analysis of the data for Al [5] showed that the IPD was actually in better agreement with an even older model due to Ecker and Kröll [8] (the EK model), though the authors of [5] were careful to note that no classical model was likely to capture all the pertinent physics. Indeed, further studies for Mg, Al, and Si in both elements and compounds have found more complex behaviour [7], as shown in Fig. 3 which are in good agreement with *ab initio* density functional theory calculations [9]. This work has aroused considerable interest, with many groups now attempting to calculate the degree of IPD in dense plasmas. A further impetus for the work has been provided by independent measurements on hotter dense plasmas, which indicate a lower degree of IPD than in the FEL experiments [10]. Interestingly, the DFT calculations hint that the IPD decreases as the temperature increases, but these calculations cannot yet attain the temperatures required to resolve the differences.

In closing this section it is also worth noting that the data shown in Fig. 2 are

extremely rich, and have also yielded information on resonance phenomenon [11] (where the k - α transitions are resonantly pumped) and on the rate of collisional ionisation within the plasma [12], though such topics are omitted here for the sake of brevity.

4. – Compression of Matter by Laser Ablation

In the previous section we considered a solid heated within 100-fsec by the FEL itself. We now consider creating HED states of matter with a few-nanosecond optical laser, and then subsequently probing these states with the FEL. Matter can be compressed statically by placing samples between two diamond anvils and applying pressure [13]. However, the pressure achievable by such means has its limits, set eventually by the ultimate strength of diamond. Whilst great advances have been made using miniature spherical nanodiamonds [14], the vast majority of work in this area is still limited to a couple of Mbar at best. On the other hand, with sufficient laser energy, Gbar pressures can be achieved with lasers (although those alongside FELs at present are limited also to a few Mbar).

A detailed quantitative model of how laser light at high intensities is absorbed by matter and produces pressure is beyond the scope of this elementary paper. However, a simple model that provides qualitative understanding (and even decent order of magnitude estimates) can be constructed as follows. First, we note that a plasma has a refractive index, μ , to light of frequency ω , given by

$$(8) \quad \mu = \sqrt{1 - \frac{\omega_p^2}{\omega^2}} \quad ,$$

where $\omega_p = \sqrt{ne^2/(\epsilon_0 m_e)}$ is the plasma frequency. Thus light can only propagate up to a certain electron density, n_c , which we call the critical density, given by $n_c = \epsilon_0 m_e \omega^2 / e^2$. A high power laser produces a plasma on the surface of the target which expands into the vacuum. The laser light deposits energy up to the critical surface, producing a hot plasma to that point. Energy must be thermally transported down from the critical surface to the target to keep ablating material. We assume a steady state situation ensues, by assuming that the flow velocity of the material at the critical surface is equal to the sound speed – it is Mach 1. That is to say $v_c \approx \sqrt{(P/\rho_c)}$. All the pieces are now in place to construct our simple model. We equate a fraction, α , of the laser intensity I to flow down the temperature gradient to sustain the ablative flow, and give rise to the rate of outflow of energy at the critical surface. That is to say,

$$(9) \quad \alpha I \approx \rho_c v_c^3 = \rho_c \left(\frac{P}{\rho_c} \right)^{3/2} \quad ,$$

where

$$(10) \quad \rho_c \approx 2m_p n_c \approx \frac{2m_p m_e \epsilon_0 \omega^2}{e^2} \quad .$$

From equations (9) and (10) we find

$$(11) \quad P = \left(\frac{8\pi^2 m_p m_e \epsilon_0 c^2}{e^2} \right)^{1/3} (\alpha I / \lambda)^{2/3} \quad .$$

For example, for light of wavelength $1\text{-}\mu\text{m}$, an irradiance of 10^{13}Wcm^{-2} , and assuming $\alpha = 0.5$, the above equation gives a pressure estimate of 2 Mbar, which is surprisingly close to the experimental result, given the crudeness of the model.

5. – Shock Compression

As the plasma ablates from the surface, from Newton's third law a pressure pulse is launched into the underlying material. As a general rule, the speed of sound increases as a function of compression such that a compression wave in a material launched by laser ablation will steepen up into a shock wave, comprising a discontinuity in density and pressure. This steepening occurs as the more compressed material is travelling faster than the less compressed material. Shock compression of matter is extremely interesting in its own right. One aspect of a shock is that the conditions behind the shock front must obey the Rankine-Hugoniot relations, which follow simply from the conservation of mass, momentum, and energy across the shock front.

Consider a shock travelling at velocity U_s through a medium with ambient conditions of a pressure P_0 and density ρ_0 and energy density E_0 . Within the material behind the shock the particles move with a velocity u_p and the density, pressure and energy density are ρ_1 , P_1 , and E_1 respectively. Conservation of mass dictates that

$$(12) \quad \rho_0 U_s = \rho_1 (U_s - u_p) \quad ,$$

whilst conservation of momentum implies that

$$(13) \quad P_1 - P_0 = \rho_0 U_s u_p \quad ,$$

and finally, conservation of energy leads to

$$(14) \quad E_1 - E_0 = \frac{1}{2}(P_1 - P_0) \left(\frac{1}{\rho_0} - \frac{1}{\rho_1} \right) \quad .$$

It should be noted that, assuming we know the ambient conditions, these three equations have five unknowns: P_1 , ρ_1 , E_1 , U_s and u_p . Therefore a measure of any two of them gives full information on the thermodynamic conditions (in terms of E_1 , P_1 and ρ_1) behind the shock. The locus of points reached by shock compression is known as the Hugoniot. It is shown schematically in PV space in Fig. 4. Note the Hugoniot lies above the cold compression curve, as the system is heated during the shock.

5.1. Pressure measurements. – The method used to deduce the pressure in the target is VISAR (velocity interferometer system for any reflector) [15]. In this system, the rear surface of the target is used as one of the reflecting surfaces in a laser-illuminated interferometer. The input laser beam is split, and a part delayed by a few nsec before being combined with an undelayed part of the original beam. Light reflected from the target experiences a Doppler shift as the surface moves as the compression wave breaks out, and this light is constantly being re-combined with the light whose frequency is determined by the conditions some short time τ earlier, where τ is the delay time. The VISAR system has some specific optical properties, which can be ascertained from reference [15], which overcome the problems of poor fringe contrast often encountered with reflection from diffusely scattering surfaces. The fringes are recorded on an optical

streak camera, and the shift in the fringes as a function of time allows a measurement of the rear surface velocity of the target.

5.2. Shock studies with X-ray FELs - Deformation. – When a crystalline solid is subjected to a shock by planar impact, huge shear stresses are induced, as the total strains (elastic plus plastic) applied to the material are fully one dimensional. This inevitably leads to some fundamental questions: how quickly can a solid material ‘flow’ to relieve these enormous shear stresses, and what are the conditions within the material on extremely short timescales? Before the advent of FELs attempts to answer these questions relied on multi-million atom molecular dynamics simulations. In the work of Bringa and co-workers [17], it was predicted that if a face-centred-cubic crystal such as copper was compressed sufficiently rapidly (on a timescale shorter than tens of femtoseconds), the ultimate elastic compressive strength of the material could be reached – that is to say at the atomic level the cubic lattice would compress in one dimension only up to a point given by the ultimate strength of the material, which corresponds to an enormous elastic compression of order 17%. [18]. The rapid compression would not give sufficient time for pre-existing defects to relieve the high stresses and strains, with the plastic strain being relieved at a rate determined by Orowan’s equation, which states that the rate of plastic strain is given by

$$(15) \quad \frac{d\epsilon_p}{dt} = N|\mathbf{b}|v \quad ,$$

where N is the number of mobile dislocations, \mathbf{b} their burgers vector, and v their velocity. Thus at very high strain rates the material would reach ultimate compressive strength, before the lattice failed by copious rapid generation of defects, and at the lattice level moving from having the unit cell compressed in one dimension, to be reduced in all three.

The experiment which demonstrated this was performed at LCLS [19], and is shown in schematic form in Fig. 5. Thin ($1\text{-}\mu\text{m}$) layers of copper were deposited on Si wafers. A compression wave, with peak pressure close to 1 Mbar, was launched in them by a roughly Gaussian 180-psec laser pulse. X-rays of energy 8 keV were diffracted from the shocked region, and could be timed w.r.t. the shock pulse to better than a psec, and then successive shots taken with the delays changed by 10 to 20 psec. The copper targets were fibre textured – that is to say normal to the target they had sub- μm grains that were preferentially oriented $\pm 3^\circ$ along the [111] direction, but random azimuthally about it. Diffraction then took place from the [111] planes. The data, alongside the simulated diffraction signal [20], is shown in Fig. 6.

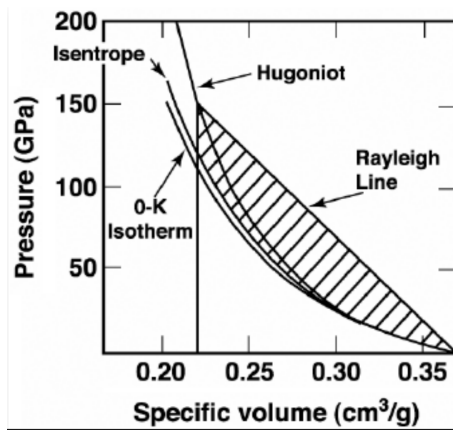


Fig. 4.: Hugoniot, isentrope and 0 K isotherm of Al from initial specific volume of crystal to specific volumes near 150 GPa pressures (McMahan 1976). Reprinted with permission from Nellis (1997), Copyright 1997, VCH Publishers. taken from [16]

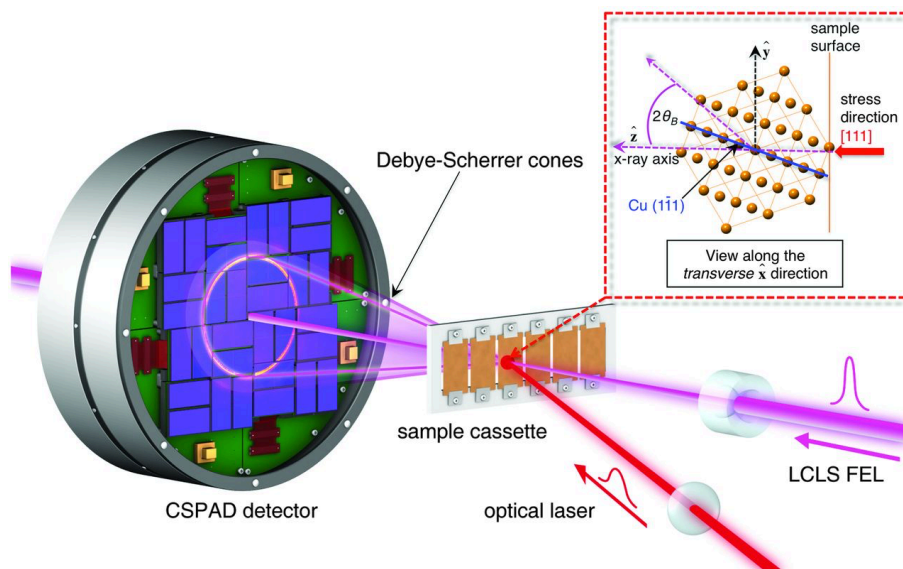


Fig. 5.: Schematic diagram of the experiment to measure the ultimate compressive strength of copper. The output of a 180-psec laser pulse focussed to a 200- μm spot launches a pressure wave into 1- μm thick fibre-textured copper. During the compression the 8 keV 100-fsec x-rays from LCLS are diffracted from the sample, forming Debye-Scherrer rings on the detector, allowing the deformation of the lattice to be recorded. Figure taken from [19].

The unshocked material scatters x-rays close to 39.5° , and diminishes in intensity as the wave traverses the sample. Early in time a new peak occurs at around 40.25° , which corresponds to 1-D elastic compression of about 17%, as predicted. On a timescale of about 60-psec, again in good agreement with original predictions, diffraction at higher angles occurs, consistent with the lattice relaxing in all three dimensions, but with a lower strain in each.

5.3. Shock studies with X-ray FELs - Phase Transitions. – As well as studying how materials deform under rapid compression, the question arises as to whether complex new phases be formed on the nanosecond timescale of these compression experiments? The short answer is yes – but with caveats that we need to consider. The most complex polymorphic shock-induced phase transition yet recorded via dynamic diffraction has been in the study of shock-compressed scandium. [21] In this experiment the Sc was shocked by laser-ablation (via a kapton overlay) to pressures in excess of 80 GPa. The diffraction data is shown in Fig. 7.

At 51.1 GPa a complex host-guest (HG) structure was observed. HG phases are remarkable states of crystalline matter, which can be thought of as one crystalline phase (the host) having periodic holes drilled through it, along which are strung 1-D chains of atoms (the guest) with a lattice-spacing completely incommensurate with that of the host. Since their initial discovery it has been noted that many materials could potentially have such structures within their phase diagram – for example aluminium is predicted to exhibit such behaviour at pressures of 3200 GPa. [22]

We note that the plot of the Hugoniot on the right hand side of Fig.7 has been obtained by deducing the density from X-ray diffraction, and the pressure using VISAR.

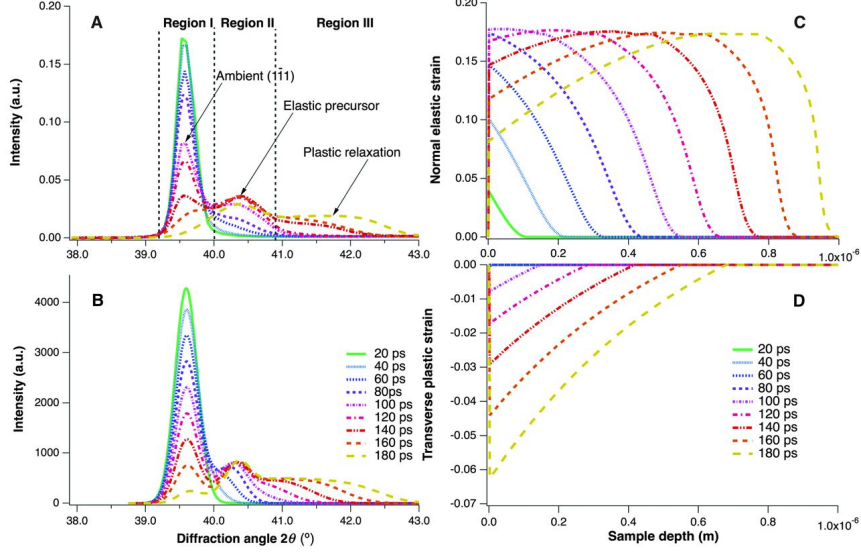


Fig. 6.: Experimental diffraction data from the experiment depicted in Fig. 5 resulting from the azimuthal integration around the Debye-Scherrer ring. The diffraction profiles are divided into three regions to illustrate the characteristic lattice response: region I, the unstrained lattice; region II, the elastically compressed lattice; and region III, the lattice exhibiting three-dimensional relaxation. a.u., arbitrary units. (B) Simulated diffraction data resulting from the calculated strain profiles, showing good agreement with experiment. (C) The modelled time-dependent normal elastic strain and (D) transverse plastic strain profiles versus sample depth using the code described in [20].

As noted in section 5, knowing these two quantities allows us to deduce the other three. It can be seen that the fractional experimental errors in the density measurement are smaller than those of the pressure. This is due to a relatively poor quality of uniformity of illumination of the drive laser, and a priority for future optical lasers sited alongside x-ray FELs will be to improve significantly the beam spatial profiles.

The phase diagram and transition pressures deduced in this work are close to those seen in static experiments. However, we note that there exist ‘sluggish’ transitions which can have significantly enthalpy barriers between phases, and given these ultrafast experiments are still very much in their infancy it remains to be seen how the phase diagram as mapped out by dynamic compression fully relates to the equilibrium diagram in many cases.

6. – X-Ray Thomson Scattering

Thus far we have considered the shock compression of matter to regimes where the sample remains solid. At higher pressures (or with x-ray heating), it can attain the plasma state. Under these conditions diffraction can still be undertaken - monitoring the x-ray scattering as a function of angle, but now the atoms are not on a crys-

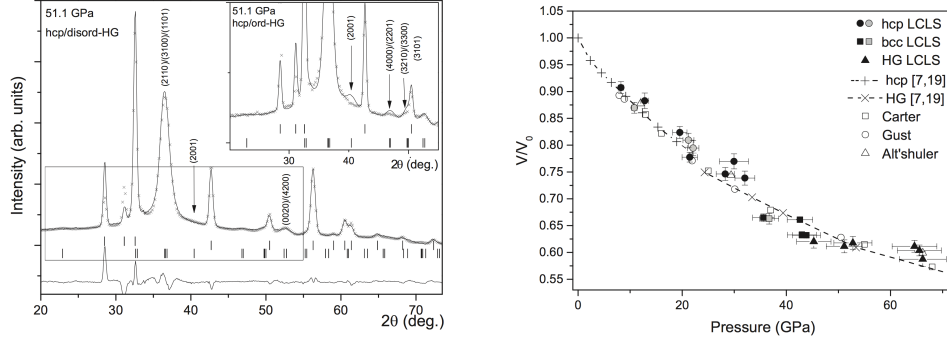


Fig. 7.: Reproduced from [21]. A two-phase (62%:38% uncompressed- hcp:disordered-HG) Rietveld fit to the diffraction profile obtained at 51.1 GPa ($\lambda=1.4089 \text{ \AA}$), with the most intense HG peaks indexed. The calculated peak positions of the best-fitting uncompressed-hcp and HG unit cells are shown by upper and lower tick marks beneath the profile. The inset shows an uncompressed-hcp/ordered-HG fit to the same profile. The additional (2001) guest-only peak, and the intensity mismatches caused by the intensities of the (2201) and (3101) guest-only peaks, are highlighted with arrows.

tal lattice, the diffracted x-rays provide a pattern corresponding more like that of a

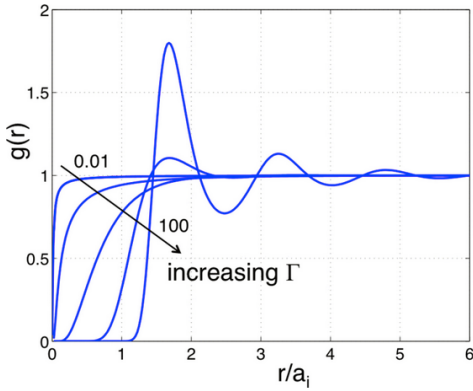


Fig. 8.: Radial distribution functions $g(r)$ (in the hypernetted-chain approximation) for a one-component plasma. taken from [23].

liquid. The diffracted x-rays now provide information on the pair distribution function, $g(r)$. If a given particle is taken to be at the origin O , and if $\rho = N/V$ is the average number density of particles, then the local time-averaged density at a distance r from O is $\rho g(r)$. The pair distribution function is a function of the degree of coupling within the plasma. As an example, Fig. 8 shows how $g(r)$ varies as we change the coupling parameter, Γ . Close to the ideal gas classical plasma (small coupling) the probability of finding particles close to a test particle is uniform. Coupling changes this, leading to the observation of shells of probability as found in a liquid. Eventually, at very high coupling, a solid would be formed.

The pair distribution factor can be measured by scattering, just like Bragg scattering from a solid. It is of great importance,

because it is related to the internal energy of the system. Care must be taken in considering the structure factor of the system, as it is often defined differently for a plasma than for a solid. A plasma physicist defines the structure factor, $S(\mathbf{k})$ as

$$(16) \quad S(\mathbf{k}) = 1 + \frac{1}{N} \left\langle \sum_{i \neq j=1}^N e^{i\mathbf{k} \cdot (\mathbf{r}_i - \mathbf{r}_j)} \right\rangle ,$$

(whereas the 1 on the right hand side is ignored by crystallographers, as then the square of structure factor is directly related to the intensity of scattered x-rays). The structure factor and pair distribution function are related by a Fourier transform

$$(17) \quad g(\mathbf{r}) - 1 = \frac{1}{N-1} \sum_{\mathbf{k}} e^{i\mathbf{k}\cdot\mathbf{r}} [S(\mathbf{k}) - 1] \quad .$$

It is beyond the level of these notes, and we refer the reader to a standard text on plasma physics, but the important point to note is that $S(\mathbf{k})$ is related to the internal energy of the system

$$(18) \quad \frac{E_{int}}{N} = \frac{3}{2} k_B T + \frac{1}{2V} \sum_{\mathbf{k} \neq 0} U_k [S(\mathbf{k}) - 1] \quad \text{where} \quad U_k = \frac{Z^2 e^2}{\epsilon_0 k^2} \quad ,$$

which in turn, via the virial theorem, is related to the pressure

$$(19) \quad \frac{P}{P^{ideal}} = 1 + \frac{1}{3} \frac{E_{int} - E_{int}^{ideal}}{N k_B T} \quad ,$$

where $P^{ideal} = N k_B T$. Hence if we could measure the structure over a significant range of k-space, we could in principle obtain information about the pressure and energy in the plasma.

Thus the experiments that can be performed with FELs comprise creating such strongly coupled plasmas by optical shock compression, and then elastically scattering the FEL pulse from them, measuring the diffraction pattern as a function of angle. An example of such data is shown in Fig. 9, where the x-rays from LCLS are scattered from a thin foil of aluminium. The Bragg peaks of the uncompressed and compressed solid are visible at the lowest pressures, and then as the material undergoes melting at high pressures, liquid diffraction features are seen that provide information on the first maximum of the $g(r)$ function, and are compared with DFT simulations. A point of importance to note is that only the first peak in $g(r)$ is being recorded, and thus measurements are not yet extending so far in reciprocal space as to fully enable comparisons with predictions of the behaviour of the higher order peaks, and allow an accurate determination of internal energy and pressure. Clearly probing with high energy x-ray laser pulses would be advantageous.

The elastically scattered x-rays as a function of angle that we have considered above give us information about the structure of the material: this is the same regime of Bragg scattering from a crystal. However, collective oscillations also take place in the plasma, from which x-rays can inelastically scatter. If electrons are displaced from the ions in a cold system then they will oscillate at the plasma frequency, which is determined by the electron density: $\omega_p = \sqrt{ne^2/\epsilon_0 m_e}$. For a cold plasma we see that such waves are non-dispersive: there is no dependence at all on k -vector. However, we note equation (4) implies that a typical thermal electron, with velocity $v_{th} = \sqrt{k_B T}$, will travel roughly a Debye length within a plasma period, so we might expect the frequency of such waves in a warm plasma to be altered when our typical electron has time to travel from a peak to a trough within the wave during one oscillation. Indeed this is the case, and a perusal of any standard plasma textbook will show that in a classical plasma this

leads to modification of the frequency of plasma waves in a warm plasma, known as the Bohm-Gross relation:

$$(20) \quad \omega^2 = \omega_p^2 + 3k^2 v_{th}^2 \quad .$$

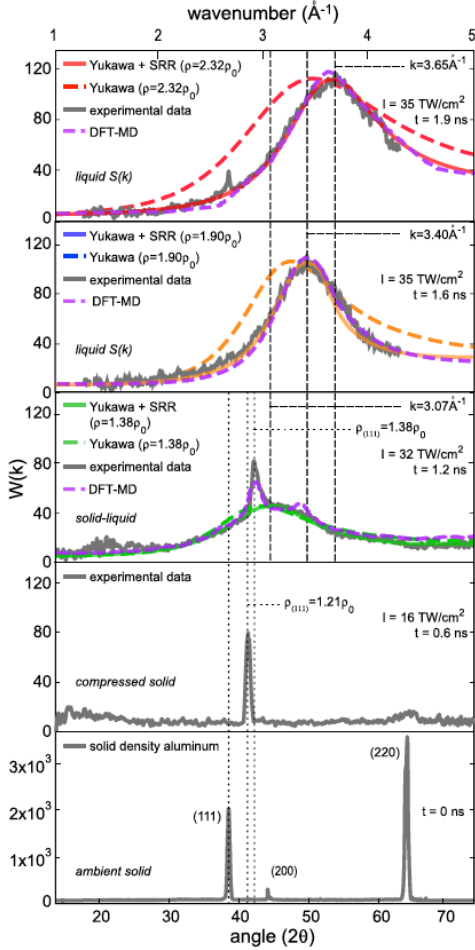


Fig. 9.: Bragg diffraction from an aluminium sample at various shock pressures as the pressure is raised from ambient, to a shock compressed solid, and finally to the liquid state, along with the inferred densities. The figure is taken from [24]

consistency with the plasma shift with a result of 1.75 ± 0.5 eV.

6.1. Quasi-Isentropic Compression. – No review of the field would be complete without mentioning that there is a growing interest in using laser ablation not just to shock-compress samples, but to compress them quasi-isentropically. The study of materials subjected to shock compression is of interest in its own right. However, in one respect

Thus x-rays incident on a plasma can also undergo inelastic scattering, where they gain or lose a quantum of the plasma energy, but now we need to monitor the energy of the scattered x-ray at a given angle, not just the fact that it has been scattered (as with elastic scattering). As the energy of the plasma wave, given by equation (20), now has terms that depend both on density and temperature, in principle both can be extracted from the change in x-ray energy. Care must be taken, however, as the derivation of the above dispersion relation is only strictly valid in the classical regime. Furthermore, the above simplified picture does not take into account damping of the plasma waves, either via collisionless or collisional damping. In practice, as we are considering non-ideal plasmas, data must be compared with more sophisticated simulations, such as those based on *ab initio* density functional theory models (see for example the work within [25]).

As an example of this inelastic scattering, Fig. 10 shows inelastic scattering, once more from shock compressed aluminium. The x-rays incident on the samples have an energy of 8 keV, and the scattered x-rays are collected by a high-efficiency Bragg crystal spectrometer. X-rays lose energy to plasmons in the system, which gives rise to the less intense peaks at lower energy, with the larger shift consistent with a compression of the aluminium from 2.7 g cm^{-3} to 6.3 g cm^{-3} . The shift in energy is dominated by the density, (i.e. the ω_p term in equation (20)), with temperature information being derived from the elastic peak amplitude, and

applying a shock in order to compress matter has a serious deficiency, the origin of which can be traced back to equation (14), in conjunction with a study of Fig. 4. We see that the total energy imparted to the material by a shock is the area of the triangle in the figure, whereas the energy required simply to compress the material is closer to the cold curve shown. The difference between the two (the straight line connecting P_0, ρ_0 and P_1, ρ_1 is known as the Rayleigh line) represents the thermal energy imparted to the material by the shock process and is shown by the hatched area: a shock is a highly entropic event that generates significant heat. So much so, that when plotted in temperature-pressure space the Hugoniot of a typical metal quickly rises above the melt curve, such that most metals melt upon shock compression somewhere between 0.5 and 3

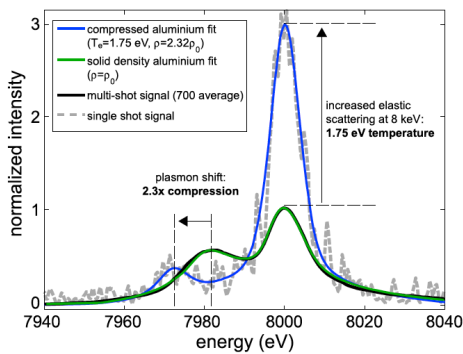


Fig. 10.: X-ray scattering spectra from laser-compressed and solid-density aluminium - see text for details. The figure is taken from [24].

Mbar (depending upon the particular metal). This is clearly disadvantageous if we wish to study solids at ultra-high pressures, which we wish to do in order to explore the phase diagram of matter into hitherto unexplored regions that may be of relevance to the conditions deep within the interiors of the plethora of exoplanets that are now being discovered on an almost daily basis. Temperature rises due to compression along an isentrope are considerably lower than those along a shock. Indeed, it can be shown by a simple argument that for most solids compression along an isentrope will result in the material staying solid, by always being below the melt line. The tenet of this argument runs as follows. The Grüneisen parameter is defined as

$$(21) \quad \gamma = \left(\frac{\partial \ln T}{\partial \ln \rho} \right)_S \equiv \left(\frac{\partial \ln \theta_D}{\partial \ln \rho} \right)_S ,$$

where θ_D is the Debye temperature of the solid:

$$(22) \quad \theta_D \approx \frac{\hbar c}{a k_B} \propto c \rho^{1/3} ,$$

where c is the speed of sound, and a the lattice spacing. The far right hand side of equation (21) follows as clearly T/θ_D is constant along an isentrope, as the number of ways that the various modes in crystal are populated cannot change along such a path.

An over-simplified but useful model of melting is given by the Lindemann criterion, which assumes that this phase transition occurs when the lattice vibrations reach an amplitude that is a certain fraction of the lattice spacing – usually taken to be about 0.1. According to the Debye model, for an rms displacement x of an atom from its equilibrium position

$$(23) \quad M \langle x^2 \rangle \omega_D^2 \approx kT ,$$

where $\hbar\omega_D = k_B\theta_D$. From the Lindemann criterion we deduce that the melt temperature, $T_m \propto a^2\theta_D^2$, which in turn from equation (22) implies

$$(24) \quad T_m \propto \theta_D^2 \rho^{-2/3} \quad ,$$

from which we deduce

$$(25) \quad \frac{d \ln T_m}{d \ln \rho} = 2 \left(\gamma - \frac{1}{3} \right) \quad .$$

From this it follows that if $\gamma > 2/3$ then the melt temperature increases with compression more quickly than the temperature along an isentrope, and thus we should be able to keep the material solid if we keep close to the isentrope. Interesting, most materials have a γ far higher than this value, providing scope for the creation of solid matter at ultra-high density.

The question that now arises is how do we compress along an isentrope, rather than a shock? The response is we must compress slowly, but how slowly? This question has been addressed by Higginbotham and co-workers [26]. If the shock were purely elastic, it would be sufficient if each part of the target were compressed on the timescale of a few phonon periods (still very fast), though care must be taken as any ramp wave tends to steepen to a shock. However, plasticity is at work to relieve the shear stress, and the authors of [26] note that the pertinent timescale to be on an isentrope is a ramp that is long compared with the natural rise time of a shock for the same pressure. It is known that the relationship between the strain rate and peak stress across a shock front obeys a fourth power law ($\dot{\epsilon}_p \propto \sigma_{\max}^4$), referred to as the Swegle-Grady relation, (though this is still far from being fully understood [27]). The pertinent timescales are a few to ten nanoseconds in most cases, and on larger laser systems than those yet put alongside extant FELs, diamond has been ramp-compressed to 50 Mbar [28], and using laser-based nanosecond x-ray sources it is known that good diffraction signals can be obtained from materials close to 12 Mbar [29] – that is to say it is known that good diffraction can be obtained using dynamic compression at these high pressures.

7. – Future Prospects and Challenges

Whilst it is not possible to do justice to all of the significant advances being made in the field of HED science using X-Ray FELs, we have tried to provide a simplified overview of some of the main types of experiments, and important results achieved to date. As we have seen, FELs have been used to isochorically heat matter, and obtain hitherto inaccessible information on the ionisation thresholds in solid density plasmas. The bright x-ray sources, shorter in duration than even the fastest phonon period, mean that diffraction patterns (elastic scattering) can be obtained from both high pressure solids and plasmas under shock compression induced by optical laser-ablation techniques. Complex phases in the solid-state have been observed on these nano-second timescales, and both elastic and inelastic scattering from dense plasmas is starting to provide useful information on their structure and equation of state.

To a large extent further advances in this field will depend heavily on improvements in both the FELs and the optical lasers used for compression. An extension of photon energy (say to 25 keV, as envisaged at the European XFEL), will be welcome as diffraction with higher momentum transfer will allow higher order peaks in the liquid/plasma pair

distribution function to be measured (necessary for any detailed information related to pressure and internal energy), and will also provide far better confidence in the inferences made about crystal structure, by increasing the number of Bragg peaks.

An optical laser with a high repetition rate (10 Hz) and 100-J per pulse energy is planned at XFEL [31], which, as can be seen from equation (11), will increase the pressures created in the targets over those given in examples within this paper. Furthermore, with sophisticated pulse shaping such a facility should allow tailored isentropic compression of the targets. In the case of such isentropic compression, a remaining significant challenge is the development of techniques to measure the temperature of the material, to provide full thermodynamic information across the phase diagram. One suggestion is to use the Debye-Waller effect – i.e. the ratio of the intensities between higher order and lower order diffraction peaks. For a reflection associated with reciprocal lattice vector \mathbf{G} , and Debye temperature θ_D , the intensity at temperature T scales as

$$(26) \quad I_G(T) \propto \exp(-A|\mathbf{G}|^2 T / \theta_D^2) \quad .$$

Interestingly, along an isentrope, the higher order reflections should actually get brighter in most cases (if $\gamma > 2/3$) for exactly the same reason why we found that the isentrope generally lies below the melt curve. An atom displaced from its equilibrium position, when compressed along an isentrope, not only reduces the magnitude of its rms displacement, but this also decreases as a fraction of the lattice spacing, thus reducing the phase mismatch for higher order peaks (i.e. $|\mathbf{G}|^2 T / \theta_D^2$ reduces upon isentropic compression if $\gamma > 2/3$ [30]). However, effective use of equation (26) will need to find methods both to infer the Debye temperature (which itself changes upon compression via γ , which itself is not truly constant), and to disentangle intensity effects related to texture (i.e. the geometric distribution of grain orientations within the sample).

8. – Summary

The advent of high brightness x-ray free electron lasers is already having significant impact in the field of High Energy Density Science. They have exquisite properties both as pumps – being able to create truly isochorically heating matter – and as probes (via both elastic and inelastic scattering). When combined with high power optical lasers, many states of HED matter can be diagnosed with a degree of precision that has hitherto proven elusive. As the number of FEL user facilities around the world grows over the next few years, with extended x-ray energy ranges and improved optical laser systems alongside them, the prospects for significant further advances in this field appear promising.

REFERENCES

- [1] *High Energy Density Physics*, () , this is the definition used by the Editors of HEDP, published by Elsevier, ISSN: 1574-1818.
- [2] ZIMMERMAN G. and MORE R., *J. Quant. Spectrosc. Radiat. Transfer*, **23** (1980) 517 .
URL <http://www.sciencedirect.com/science/article/pii/0022407380900552>
- [3] VINKO S. M., CIRICOSTA O., CHO B. I., ENGELHORN K., CHUNG H. K., BROWN C. R. D., BURIAN T., CHALUPSKY J., FALCONE R. W., GRAVES C., HAJKOVA V., HIGGINBOTHAM A., JUHA L., KRZYWINSKI J., LEE H. J., MESSERSCHMIDT M., MURPHY C. D., PING Y., SCHERZ A., SCHLOTTER W., TOLEIKIS S., TURNER J. J., VYSIN L., WANG T., WU B., ZASTRAU U., ZHU D., LEE R. W., HEIMANN P. A., NAGLER B. and

- WARK J. S., *Nature*, **482** (2012) 59.
URL <http://dx.doi.org/10.1038/nature10746>
- [4] STEWART J. C. and PYATT JR. K. D., *Astrophys. J.*, **144** (1966) 1203.
- [5] CIRICOSTA O., VINKO S. M., CHUNG H.-K., CHO B.-I., BROWN C. R. D., BURIAN T., CHALUPSKÝ J., ENGELHORN K., FALCONE R. W., GRAVES C., HÁJKOVÁ V., HIGGINBOTHAM A., JUHA L., KRZYWINSKI J., LEE H. J., MESSERSCHMIDT M., MURPHY C. D., PING Y., RACKSTRAW D. S., SCHERZ A., SCHLOTTER W., TOLEIKIS S., TURNER J. J., VYSIN L., WANG T., WU B., ZASTRAU U., ZHU D., LEE R. W., HEIMANN P., NAGLER B. and WARK J. S., *Phys. Rev. Lett.*, **109** (2012) 065002.
URL <http://link.aps.org/doi/10.1103/PhysRevLett.109.065002>
- [6] CIRICOSTA O., VINKO S. M., CHUNG H.-K., JACKSON C., LEE R. W., PRESTON T. R., RACKSTRAW D. S. and WARK J. S., *Physics of Plasmas*, **23** (2016) 022707.
URL <http://dx.doi.org/10.1063/1.4942540>
- [7] CIRICOSTA O., VINKO S. M., BARBREL B., RACKSTRAW D. S., PRESTON T. R., BURIAN T., CHALUPSKÝ J., CHO B. I., CHUNG H.-K., DAKOVSKI G. L., ENGELHORN K., HÁJKOVÁ V., HEIMANN P., HOLMES M., JUHA L., KRZYWINSKI J., LEE R. W., TOLEIKIS S., TURNER J. J., ZASTRAU U. and WARK J. S., *Nature Communications*, **7** (2016) 11713 EP , article.
URL <http://dx.doi.org/10.1038/ncomms11713>
- [8] ECKER G. and KRÖLL W., *Phys. Fluids*, **6** (1963) 62.
- [9] VINKO S. M., CIRICOSTA O. and WARK J. S., *Nat. Commun.*, **5** (2014) 3533 EP .
URL <http://dx.doi.org/10.1038/ncomms4533>
- [10] HOARTY D. J., ALLAN P., JAMES S. F., BROWN C. R. D., HOBBS L. M. R., HILL M. P., HARRIS J. W. O., MORTON J., BROOKES M. G., SHEPHERD R., DUNN J., CHEN H., VON MARLEY E., BEIERSDORFER P., CHUNG H. K., LEE R. W., BROWN G. and EMIG J., *Phys. Rev. Lett.*, **110** (2013) 265003.
URL <https://link.aps.org/doi/10.1103/PhysRevLett.110.265003>
- [11] CHO B. I., ENGELHORN K., VINKO S. M., CHUNG H.-K., CIRICOSTA O., RACKSTRAW D. S., FALCONE R. W., BROWN C. R. D., BURIAN T., CHALUPSKÝ J., GRAVES C., HÁJKOVÁ V., HIGGINBOTHAM A., JUHA L., KRZYWINSKI J., LEE H. J., MESSERSCHMIDT M., MURPHY C., PING Y., ROHRINGER N., SCHERZ A., SCHLOTTER W., TOLEIKIS S., TURNER J. J., VYSIN L., WANG T., WU B., ZASTRAU U., ZHU D., LEE R. W., NAGLER B., WARK J. S. and HEIMANN P. A., *Phys. Rev. Lett.*, **109** (2012) 245003.
URL <https://link.aps.org/doi/10.1103/PhysRevLett.109.245003>
- [12] VINKO S. M., CIRICOSTA O., PRESTON T. R., RACKSTRAW D. S., BROWN C. R. D., BURIAN T., CHALUPSKÝ J., CHO B. I., CHUNG H. K., ENGELHORN K., FALCONE R. W., FIOKOVININI R., HÁJKOVÁ V., HEIMANN P. A., JUHA L., LEE H. J., LEE R. W., MESSERSCHMIDT M., NAGLER B., SCHLOTTER W., TURNER J. J., VYSIN L., ZASTRAU U. and WARK J. S., *Nat. Commun.*, **6** (2015) 6397 EP .
URL <http://dx.doi.org/10.1038/ncomms7397>
- [13] JAYARAMAN A., *Rev. Mod. Phys.*, **55** (1983) 65.
URL <https://link.aps.org/doi/10.1103/RevModPhys.55.65>
- [14] DUBROVINSKAIA N., DUBROVINSKY L., SOLOPOVA N. A., ABAKUMOV A., TURNER S., HANFLAND M., BYKOVA E., BYKOV M., PRESCHER C., PRAKAPENKA V. B., PETITGIRARD S., CHUVASHOVA I., GASHAROVA B., MATHIS Y.-L., ERSHOV P., SNIGIREVA I. and SNIGIREV A., *Sci Adv*, **2** (2016) e1600341, 1600341[PII].
URL <http://www.ncbi.nlm.nih.gov/pmc/articles/PMC4956398/>
- [15] BARKER L. M. and HOLLENBACH R. E., *Journal of Applied Physics*, **43** (1972) 4669.
URL <http://dx.doi.org/10.1063/1.1660986>
- [16] NELLIS W. J., *Reports on Progress in Physics*, **69** (2006) 1479.
URL <http://stacks.iop.org/0034-4885/69/i=5/a=R05>
- [17] BRINGA E. M., ROSOLANKOVA K., RUDD R. E., REMINGTON B. A., WARK J. S., DUCHAINEAU M., KALANTAR D. H., HAWRELIAK J. and BELAK J., *Nature materials*, **5** (2006) 805.

- [18] DUPONT V. and GERMANN T. C., *Phys. Rev. B*, **86** (2012) 134111.
URL <http://link.aps.org/doi/10.1103/PhysRevB.86.134111>
- [19] MILATHIANAKI D., BOUTET S., WILLIAMS G. J., HIGGINBOTHAM A., RATNER D., GLEASON A. E., MESSERSCHMIDT M., SEIBERT M. M., SWIFT D. C., HERING P., ROBINSON J., WHITE W. E. and WARK J. S., *Science (New York, N.Y.)*, **342** (2013) 220.
URL <http://www.sciencemag.org/content/342/6155/220.abstract>
- [20] WARK J. S., HIGGINBOTHAM A., MILATHIANAKI D. and GLEASON A., *Journal of Physics: Conference Series*, **500** (2014) 152016.
- [21] BRIGGS R., GORMAN M. G., COLEMAN A. L., MCWILLIAMS R. S., MCBRIDE E. E., MCGONEGLE D., WARK J. S., PEACOCK L., ROTHMAN S., MACLEOD S. G., BOLME C. A., GLEASON A. E., COLLINS G. W., EGGERT J. H., FRATANDUONO D. E., SMITH R. F., GALTIER E., GRANADOS E., LEE H. J., NAGLER B., NAM I., XING Z. and MCMAHON M. I., *Phys. Rev. Lett.*, **118** (2017) 025501.
URL <https://link.aps.org/doi/10.1103/PhysRevLett.118.025501>
- [22] PICKARD C. J. and NEEDS R. J., *Nat Mater*, **9** (2010) 624.
URL <http://dx.doi.org/10.1038/nmat2796>
- [23] STANTON L. G. and MURILLO M. S., *Phys. Rev. E*, **93** (2016) 043203.
URL <https://link.aps.org/doi/10.1103/PhysRevE.93.043203>
- [24] GLENZER S. H., FLETCHER L. B., GALTIER E., NAGLER B., ALONSO-MORI R., BARBREL B., BROWN S. B., CHAPMAN D. A., CHEN Z., CURRY C. B., FIUZA F., GAMBOA E., GAUTHIER M., GERICKE D. O., GLEASON A., GOEDE S., GRANADOS E., HEIMANN P., KIM J., KRAUS D., MACDONALD M. J., MACKINNON A. J., MISHRA R., RAVASIO A., ROEDEL C., SPERLING P., SCHUMAKER W., TSUI Y. Y., VORBERGER J., ZASTRAU U., FRY A., WHITE W. E., HASTING J. B. and LEE H. J., *Journal of Physics B: Atomic, Molecular and Optical Physics*, **49** (2016) 092001.
URL <http://stacks.iop.org/0953-4075/49/i=9/a=092001>
- [25] GERICKE D. O., VORBERGER J., WÜNSCH K. and GREGORI G., *Phys. Rev. E*, **81** (2010) 065401.
URL <https://link.aps.org/doi/10.1103/PhysRevE.81.065401>
- [26] HIGGINBOTHAM A., HAWRELIAK J., BRINGA E. M., KIMMINAU G., PARK N., REED E., REMINGTON B. A. and WARK J. S., *Phys. Rev. B*, **85** (2012) 024112.
URL <https://link.aps.org/doi/10.1103/PhysRevB.85.024112>
- [27] GRADY D. E., *Journal of Applied Physics*, **107** (2010) .
URL <http://scitation.aip.org/content/aip/journal/jap/107/1/10.1063/1.3269720>
- [28] SMITH R. F., EGGERT J. H., JEANLOZ R., DUFFY T. S., BRAUN D. G., PATTERSON J. R., RUDD R. E., BIENER J., LAZICKI A. E., HAMZA A. V., WANG J., BRAUN T., BENEDICT L. X., CELLIERS P. M. and COLLINS G. W., *Nature*, **511** (2014) 330.
URL <http://dx.doi.org/10.1038/nature13526>
- [29] LAZICKI A., RYGG J. R., COPPARI F., SMITH R., FRATANDUONO D., KRAUS R. G., COLLINS G. W., BRIGGS R., BRAUN D. G., SWIFT D. C. and EGGERT J. H., *Phys. Rev. Lett.*, **115** (2015) 075502.
URL <https://link.aps.org/doi/10.1103/PhysRevLett.115.075502>
- [30] MURPHY W. J., HIGGINBOTHAM A., WARK J. S. and PARK N., *Phys. Rev. B*, **78** (2008) 014109.
URL <https://link.aps.org/doi/10.1103/PhysRevB.78.014109>
- [31] BANERJEE S., ERTEL K., MASON P., PHILLIPS J., GREENHALGH J. and COLLIER J., *Proc. SPIE*, **8780** (2013) 878006.
URL <http://dx.doi.org/10.1117/12.2016611>